Supplementary Material

Supplementary Section 1: *Compilation of the old and new $\delta^{15}N$ datasets for EDC*

The compilation is interpolated at a fine age scale (every 100 years) and smoothed through a 5,000-year running average (blue line in Fig. S1). Including the data measured at the University of Bern exerts a small influence on the compiled $\delta^{15}N$ record over the Marine Isotope Stage 8 (see orange line in Fig. S1).

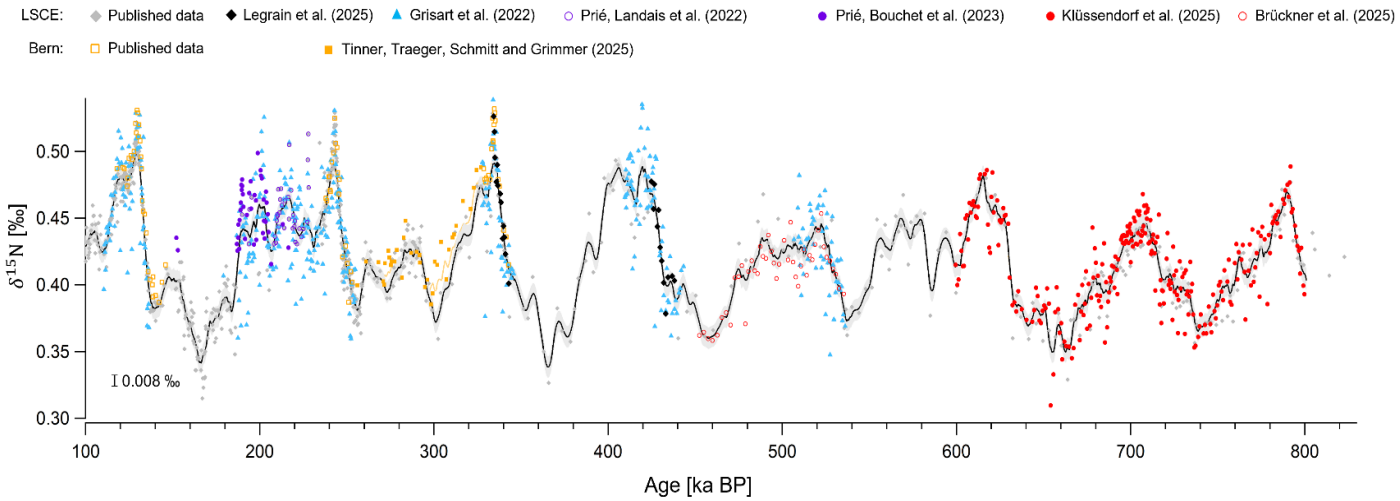

Figure S1 *Compilation of the old and new $\delta^{15}N$ datasets for EDC between 800 and 100 ka BP. The 5,000-year-running average compilation is shown by the black curve. The grey envelope depicts 1σ error (±0.008‰; also depicted by a vertical bar at the bottom left-hand corner). The compilation includes published datasets [1–4] (grey diamonds); data published in the companion paper by Legrain et al. (submitted) (black diamonds) and data presented in this study shown by: (i) blue triangles (collected over 2020-2022 by Antoine Grisart and others); (ii) purple circles (collected in 2022 by Frédéric Prié and others); (iii) purple dots (collected in 2023 by Marie Bouchet and others); (iv) red dots (collected over 2023-2025 by Anna Klüssendorf et al.); and (v) red circles (collected over 2024-2025 by Louisa Brückner and Claire-Mathilde Stücki). For comparison, $\delta^{15}N$ measurements on the EDC ice core made at the University of Bern are shown by empty orange squares [5] and filled orange squares (collected over 2025 by Patrice Tinner, Henrique Traeger, Jochen Schmitt and Markus Grimmer). The 5,000-year-smoothed compilation including the Bern measurements is shown by the orange curve.*

Supplementary Section 2: Comparison of $\delta^{15}N$ versus δD measurements

The δD series of Landais et al.[6] are interpolated so that we have series with δ^{15}N and δD on a coherent timescale. The apparent positive correlation between the δ^{15}N and δD signals is confirmed by the linear regression obtained between the two signals: $\delta^{15}N = 0.00180 + 1.18 \pm 0.02 \times \delta D \pm 0.00004$ (correlation coefficient $r^2 = 0.67$).

Following the strategy of Dreyfus et al.[2], the regression is repeated with a 400-year smoothed (running mean) δD record before running again the interpolation on the δ^{15}N age levels. There is only a marginal improvement to the fit which accounts for 68% of the δ^{15}N variability using the same linear relationship within the uncertainty range (Table S1). Therefore, the centennial scale variations in the δD signal do not help explain the full δ^{15}N variance.

Table S1. *Linear regression between $\delta^{15}N$ and δD. The linear fit is performed using a least square algorithm. The deuterium content is either directly interpolated onto $\delta^{15}N$ ages or smoothed using a 400-year running average to get rid of the centennial scale variability beforehand.*

δ^{15}N versus	**Linear relationship**	**Correlation coefficient r^2**
δD interpolated on δ^{15}N ages	$\delta^{15}N = 1.18 \pm 0.02 + 0.00180 \pm 0.00004 \times \delta D$	0.67
δD 400-year smoothed then interpolated on δ^{15}N ages	$\delta^{15}N = 1.20 \pm 0.02 + 0.00182 \pm 0.00004 \times \delta D$	0.68

Supplementary Section 3: Mismatch between measured and modeled $\delta^{15}N$

The main firn densification model used in this study has been tuned to fit the δ^{15}N profile over the last deglaciation by Bréant et al.[3].

Possible explanations for large mismatches observed during glacial period at high obliquity could be:

(i) The existence of a convective zone in the upper part of the firn, where atmospheric air is mixed and no molecular diffusion occurs. With the existence of a convective zone, the diffusive zone thickness would be different from the LID. If a convective zone develops in the upper firn and if its thickness varies in time, as the δ^{15}N only reflects the diffusive zone thickness, the δ^{15}N would not be proportional to the firn thickness (i.e., LID) anymore.

(ii) Inadequate physical parameterization of the firn model and/or inaccurate climatic scenarios used as input of the firn model (snow accumulation rate, temperature anomaly at the ice sheet surface, dust content in the firn).

(i) Convective zone

Some studies suggested that wind activity could be responsible for the existence of a convective zone in the upper part of the firn during glacial periods, thus challenging the linearity of the relationship between $\delta^{15}N$ data and firn thickness, and preventing the firn model from forecasting $\delta^{15}N$ values [2,7]. Previous work based on dating constraints over the last glacial period (MIS 3) have however revealed that the possibility of significant convective zones at Dome C is improbable [8–10].

(ii) Model configuration

We varied the physics of the densification model as well as the temperature and accumulation rate scenarios as input of the models based on existing studies (Table S2).

Varying the physics in the model

We varied the physics of the firn densification model either using the configuration described in Bréant et al.[3], in Arnaud et al.[11] or in Herron and Langway [12]. We will refer to these configurations respectively as B, A and HL.

Varying the forcing scenarios

We force the firn densification model with different histories of 1) temperature, 2) accumulation and 3) dust flux.

1. Air temperature anomaly with respect to present-day at the ice sheet surface

The A and HL parameterizations of the model are tested with two temperature scenarios. The configuration A-T1 and HL-T1 are forced by a temperature history based on δD corrected for source effects using d-excess [6] (see orange line in Fig. S2) on which two different δD – temperature slopes are applied. The T1 scenario uses the spatial slope obtained in Masson-Delmotte et al.[13] leading to a temperature difference between the pre-industrial period and the LGM ($\Delta T_{PI\text{-}LGM}$) of 9°C. The T2 scenario is based on the temporal relationship obtained in Buizert et al.[14] with a $\Delta T_{PI\text{-}LGM}$ of ~5°C. For these different scenarios, it is assumed that the evolution of surface temperature is strongly correlated

with the evolution of the δD.

2. Snow accumulation rate history

The parameterization B of the model is tested with three accumulation scenarios derived from the δD record. In the B-5000 configuration, the snow accumulation rate scenario is inferred from δD and statistically adjusted to comply with AICC2023 age constraints[15]. In the B-A1 configuration, the accumulation rate is inferred from δD measurements and adjusted to respect AICC2012 chronology [10]. In the B-A2 configuration, the history of the local snow accumulation rate is yielded by the GRISLI ice sheet model [16]. It is therefore constrained by past histories of local air temperature inferred from ice core δD data and of sea surface temperature derived from marine δ^{18}O data.

These three alternative estimates of the accumulation rate scenarios only differ by up to 0.5 cm i.e. yr^{-1} which is below the maximum uncertainty of the accumulation rate reconstruction (0.9 cm i.e. yr^{-1} ; [15]).

3. Dust content in the firn

The parameterization B of the model is tested with no dust (B-dust0) as well as with the calcium ions record of Lambert et al.[17] for configuration B-5000.

To compare the modeled and observed δ^{15}N, the modeled δ^{15}N series are interpolated every 100 years and smoothed using a 5,000-year running average to remove the millennial-scale variability (panel a in Fig. S2). Two alternative smoothing are tested for comparison: without smoothing (configuration B) and smoothed over a 2,500-year interval (configuration B-2500). The linear correlation coefficient *r* between the modeled scenarios and the measurements is calculated over a sliding 25-kyr interval (panel b in Fig. S2). A sliding interval of 10 kyr is also used for comparison for configuration B.

Neither modification of the firn physics nor use of different available temperature, accumulation rate or dust input scenario can explain the δ^{15}N model-data mismatch.

Table S2. *Parameters for the different configurations of the firn densification model. For the configuration B, the sliding correlation coefficient is calculated over intervals of 10 kyr and 25 kyr. The δ^{15}N scenario is either non smoothed (B) or smoothed over an interval of 5000 years (B-5000). For the rest of the configurations, the interval of 25 kyr is kept and the smoothing over a 5,000-year interval is kept. // means that the parameter is the same from one test the following one. The text written in bold indicates the parameter that is changed from one test to the following one.*

Configuration	Physics	Temperature anomaly	Snow accumulation rate	Dust [Ca^{2+}]
B-5000	Bréant et al.[3]	inferred from δD and corrected from source effects [6]	inferred from δD and tuned to respect AICC2023 age constraints [15]	Lambert et al. [17]
HL-T1 (varying model physics wrt B)	**Herron and Langway [12]**	//	//	
HL-T2 (varying temperature forcing wrt HL-T1)	Herron and Langway [12]	**ΔT_{PD-LGM} divided by 2 as per Buizert et al. [14]**	//	
A-T1 (varying model physics wrt B)	**Arnaud et al. [11]**	//	inferred from δD and tuned to respect AICC2023 age constraints [15]	//
A-T2 (varying temperature forcing wrt A-T1)	Arnaud et al. [11]	**ΔT_{PD-LGM} divided by 2 as per Buizert et al. [14]**	//	//
B-dust0 (varying dust parameter wrt B)	Bréant et al.[3]	inferred from δD and corrected from source effects [6]	//	**No dust**
B-A1 (varying accumulation forcing wrt B)	//	//	**inferred from δD and tuned to respect AICC2012 constraints**[10]	//
B-A2 (varying accumulation forcing wrt B)	//	//	**Inferred from the GRISLI ice sheet model (Quiquet, Dumas)**	//

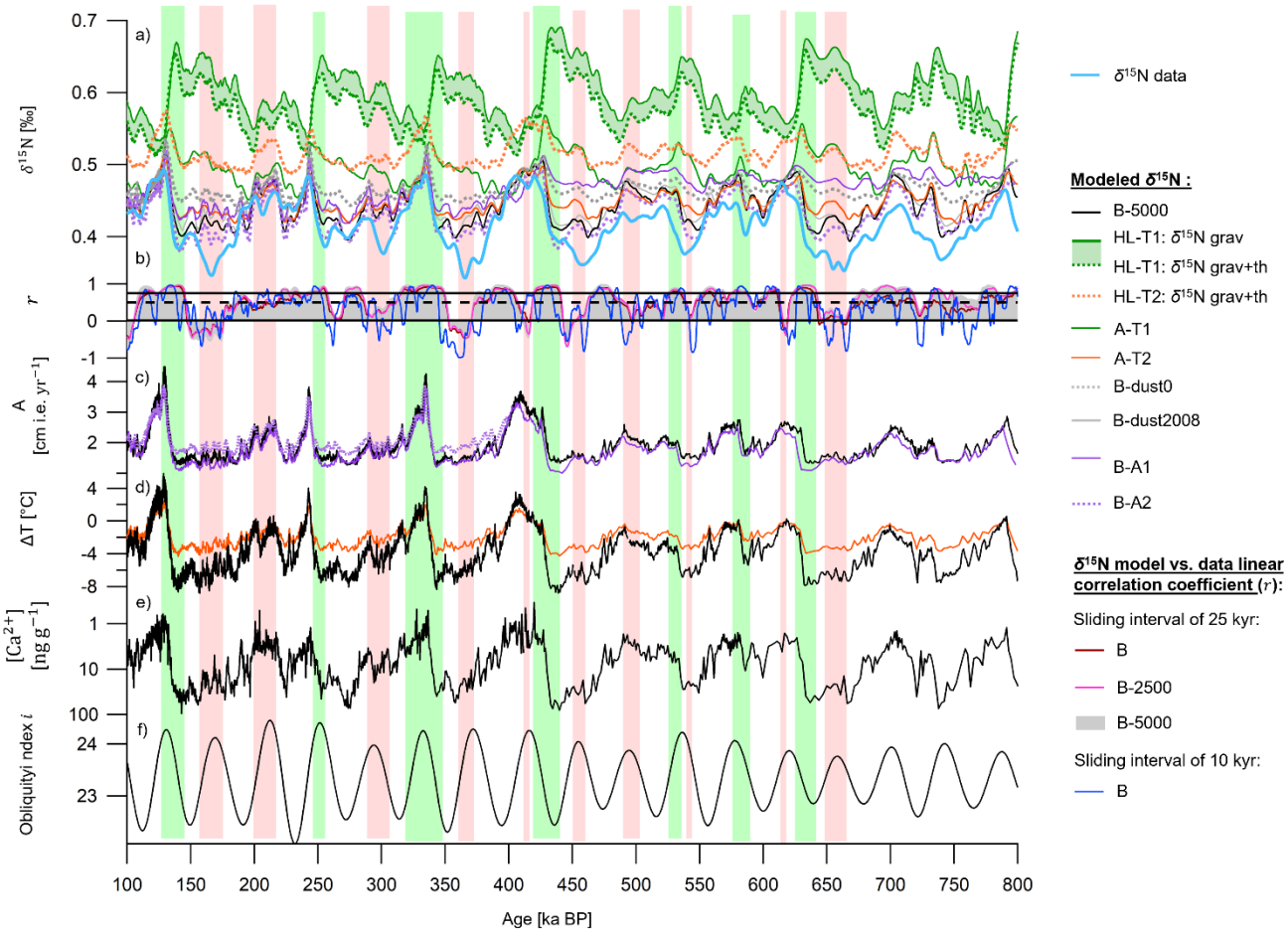

Figure S2 *Evolution of the $\delta^{15}N$ model-data mismatch depending on the model configuration. a) Modeled $\delta^{15}N$ as per various configurations of the firn model (Table S2). For HL, only $\delta^{15}N_{grav}$ can be modeled. To yield the total $\delta^{15}N$, we added the thermal contribution ($\delta^{15}N_{th}$) calculated using B-T1 and B-T2. The effect of $\delta^{15}N_{th}$ is shown for HL-T1 by the green color between the green dashed and plain curves (see legend). b) Correlation coefficient of the linear regression $\delta^{15}N$ data versus the modeled $\delta^{15}N$ (configuration B) using different time intervals for smoothing or for linear regression (see legend). The different histories of c) snow accumulation rate (A), d) site temperature anomaly with respect to present-day (ΔT) and e) dust content $[Ca^{2+}]$[17] (f) Obliquity parameter. Red shaded areas indicate time intervals wider than 5,000 years where $-0.5 < r < 0.5$ and during which the model-data mismatch exceeds 0.04 ‰ (1σ of the $\delta^{15}N$ data). Green shaded areas frame deglaciations where $r > 0.75$.*

Supplementary section 4: *LOVECLIM simulations*

Model set-up

To understand the processes that could lead to a different atmospheric circulation pattern as a function of obliquity, numerical experiments are performed with the Earth system model LOVECLIM. LOVECLIM includes a free surface primitive equation ocean model with a horizontal resolution of 3°x3° and 20 unevenly spaced vertical levels, a dynamic/thermodynamic sea-ice model, a quasi-geostrophic T21 atmospheric model, a dynamic global vegetation model (DGVM) and a marine carbon cycle model. The DGVM used, VECODE (Vegetation Continuous Description model), simulates the vegetation structure, and associated terrestrial carbon reservoirs [18]. A transient simulation of the last 140 kyr is performed by forcing the model with time varying orbital parameters [19], atmospheric greenhouse gases[20] and changes in continental ice sheets. The penultimate deglaciation (140-120 ka) follows the PMIP4 protocol[21,22]. Between 120 and 21 ka, changes in continental ice sheets are taken from Abe Ouchi et al. [23] (using the IcIES ice sheet model) and Menviel et al. [24], while from 21 ka, continental ice sheet changes are derived from ICE5G [25,26]. The Bering strait is gradually closed at 70 ka and kept closed until the early Holocene.

From that transient experiment, two 49ka experiments are run because the obliquity is maximum at 49 ka (24.3°). For the standard 49ka experiment (high obliquity), the model is run for 4000 years with prognostic atmospheric CO_2 concentration and under constant 49 ka boundary conditions. The last 1000 years of this experiment are kept for our analysis. To assess the impact of low obliquity, another experiment is run under 49 ka boundary conditions but with an obliquity of 22.1°, which represents the minimum obliquity value of the last 500 ka. This low obliquity experiment starts from the transient state and is first run for 4000 years with a constant atmospheric CO_2 concentration of 204 ppm, after which it is run with prognostic CO_2 for 2000 years.

High vs low obliquity at 49 ka

Annual and seasonal temperatures and precipitations at high (true value at 49 ka) and low obliquity averaged over 65-77°S; 100-140°E are reported in Table S3.

The temperature weighted by the amount of seasonal precipitation is calculated as per: $T_w = (T_{DJF}PP_{DJF}+T_{MAM}PP_{MAM}+T_{JJA}PP_{JJA}+T_{SON}PP_{SON})/(PP_{DJF}+PP_{MAM}+PP_{JJA}+PP_{SON})$ for low and high obliquity contexts. T_{DJF} and PP_{DJF} refer to the austral summer temperature and precipitation, averaged over the months of December, January and February. T_{MAM} and PP_{MAM} are averaged over March, April and May; T_{JJA} and PP_{JJA} over June, July and August; and T_{SON} and PP_{SON} over September, October and November.

ΔT is the temperature difference between high and low obliquity. The ΔT value for the weighted temperature (Table S3) is lower (**+1.7°C**) compared to the ΔT value calculated with mean annual temperature (**+2°C**) due to the obliquity-induced decrease in summer snowfall.

Table S3. *Annual and seasonal temperature and precipitation amount estimated by LOVECLIM model under 49 ka boundary conditions at high (true) and low obliquity averaged over 65-77°S ; 100-140°E. The difference in temperature and precipitation amounts suggested by the LOVECLIM model over an obliquity increase are respectively given in the lines named ΔT (high – low) and ΔA (high – low). The weighted temperature is defined for low and high obliquity as per* $T_w = (T_{DJF}PP_{DJF} + T_{MAM}PP_{MAM} + T_{JJA}PP_{JJA} + T_{SON}PP_{SON})/(PP_{DJF} + PP_{MAM} + PP_{JJA} + PP_{SON})$.

	Temperature *(°C)*					
	Annual	**DJF**	MAM	JJA	SON	Weighted T_w
High obliquity (24.3°)	-32.2	-21.35	-33.95	-39.02	-34.56	-31.06
Low obliquity (22.1°)	-34.2	-26.1	-35.4	-39.5	-35.8	-32.75
ΔT (high–low)	**+2°C**					**+1.7°C**
	Precipitation ***(water + snow; in w.e. cm yr^{-1})***					
High obliquity (24.3°)	26.07	32.8	30.1	19.5	21.9	
Low obliquity (22.1°)	27.2	39.9	28	17.8	23.2	
ΔA (high–low)	**-5%**	**-18%**				

Transient simulation over the past 140 kyr

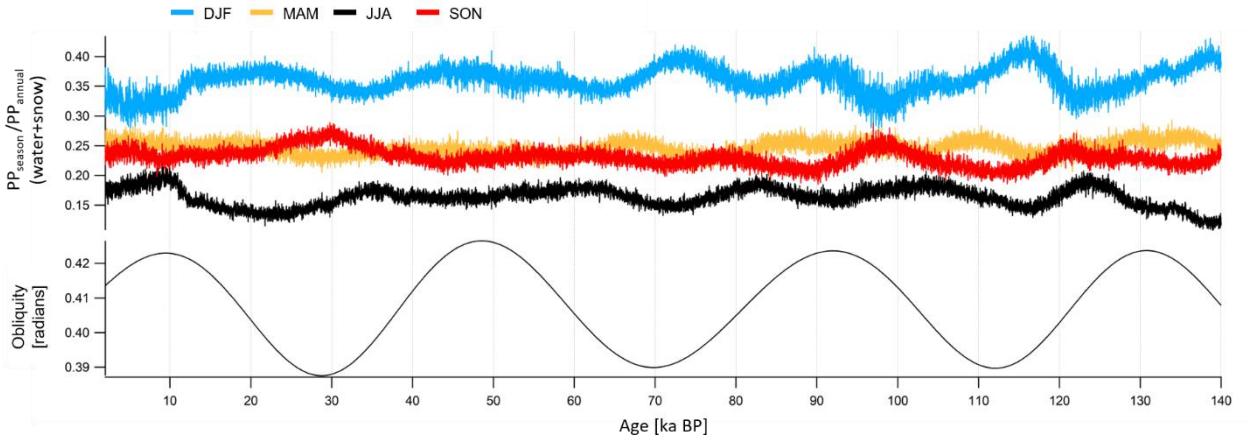

Figure S4 *Relative contribution of seasonal precipitation to the annual amount at Dome C (in the region 70-77°S; 100-140°E) over the past 140 kyr. PP_{DJF}/PP_{ann} (blue), PP_{MAM}/PP_{ann} (orange), PP_{JJA}/PP_{ann} (black), PP_{SON}/PP_{ann} (red) from LOVECLIM transient simulations. Their evolution is shown with respect to the obliquity parameter shown in bottom panel. The obliquity maximum at 49 ka coincides with one of the local maxima in the austral summer contribution.*

<u>Supplementary section 5:</u> Obliquity influence on local climate and tracers

Obliquity influence on $\delta^{15}N$ via changes in temperature and snow accumulation rate

To evaluate the possible influence of obliquity on $\delta^{15}N$, we ran several simulations of the firn densification model using new temperature and snow accumulation rate scenarios inspired by the LOVECLIM simulation (Supplementary section 4). We used two configurations of the firn densification model: A and B (Arnaud et al.[11] and Bréant et al.[3]) to eliminate a potential bias due to the physics considered in the model.

(i) Temperature

The model of Bréant et al.[3] indicates a decrease of 0.03 ‰ in $\delta^{15}N$ scenario due to an increase of 2°C in mean annual temperature when applied to MIS 6. For the same forcing, the models of Arnaud et al.[11] and of Herron and Langway[12] predict a decrease by 0.04 ‰ and 0.07 ‰ respectively in $\delta^{15}N$ (orange frame in Fig. S5). Thus, regardless of the physics involved in the model, a +2°C increase in temperature at Dome C could be responsible for a decrease in $\delta^{15}N$ between 0.03 and 0.07 ‰. We report this estimate in the panel b of Fig. 2 in the main text.

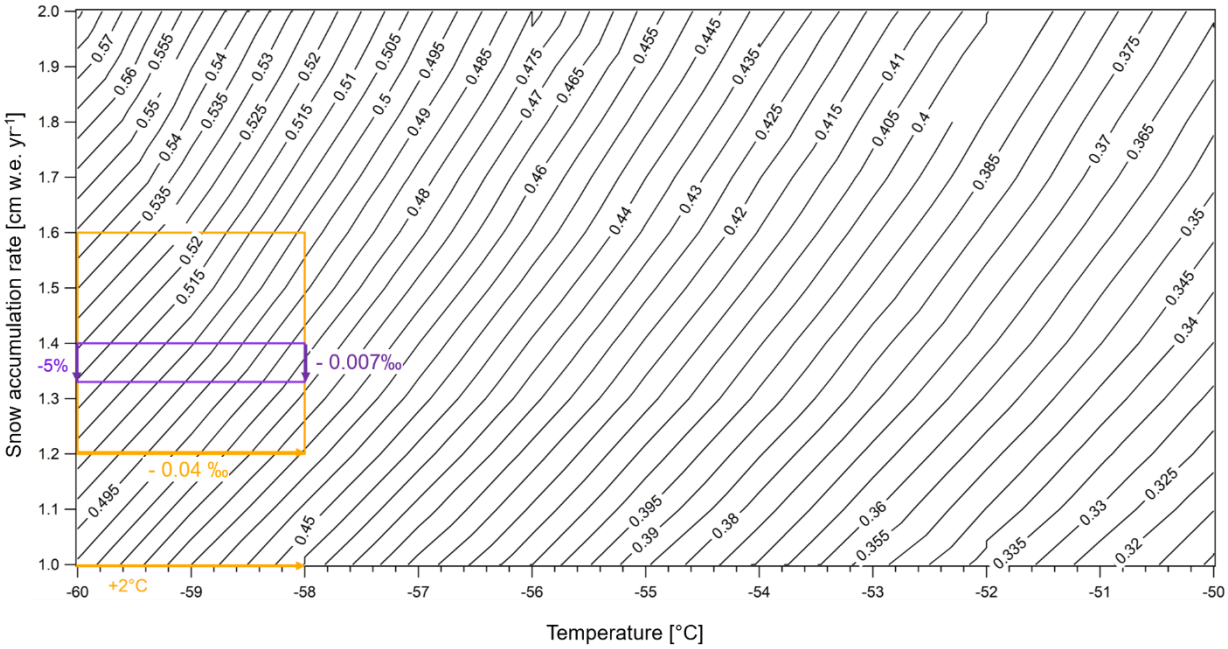

Figure S5 *Predicted $\delta^{15}N$ value as per the Arnaud et al.[11] model in function of site temperature and snow accumulation rate. The orange arrow depicts a 2°C-increase in temperature from -60°C to -58°C (on x-axis) and the orange rectangle frames the corresponding decrease in the $\delta^{15}N$ for a snow accumulation rate value between 1.6 and 1.2 cm w.e. per year. The purple arrow depicts the 5% decrease in snow accumulation rate from 1.4 to 1.33 cm w.e. yr^{-1} and associated decrease in $\delta^{15}N$ for a site temperature comprised between -58 and -60°C.*

(ii) Snow accumulation rate

The decrease in modeled $\delta^{15}N$ caused by a high-obliquity-driven 5%-decrease in mean annual snowfall is about 0.01 ‰ when applied to MIS 6 as per the Arnaud et al.[11] and the Bréant et al.[3] models. It is about 0.02 ‰ as per the model of Herron and Langway[12]. This order of magnitude for the $\delta^{15}N$ decrease (from 0.01 to 0.02 ‰) is reported in the panel b of Fig. 2 in the main text.

***Supplementary Section 6*: Reduction of the $\delta^{15}N$ model-data mismatch using the obliquity-modulated climatic scenarios**

Table S4. *Maximum relative reduction in the $\delta^{15}N$ data-model mismatch values for glacial periods (MIS 6, 8, 10, 12, 14, 16 and 18) at obliquity maxima. The reduction is estimated using the two indexes i' and i''. Only the largest value is reported in the table. *The value obtained when considering also $\delta^{15}N$ data measured at the University of Bern for the global curve.*

	MIS 6	**MIS 8**	**MIS 10**	**MIS 12**	**MIS 14**	**MIS 16**	**MIS 18**	**Average**
Maximum relative reduction in the model-data mismatch	~170 ka BP	~295 ka BP	~370 ka BP	~455 ka BP	~535 ka BP	~660 ka BP	~745 ka BP	
	-85%	-65% -85%*	-100%	-90%	-100%	-60%	-95%	-85% -88%*

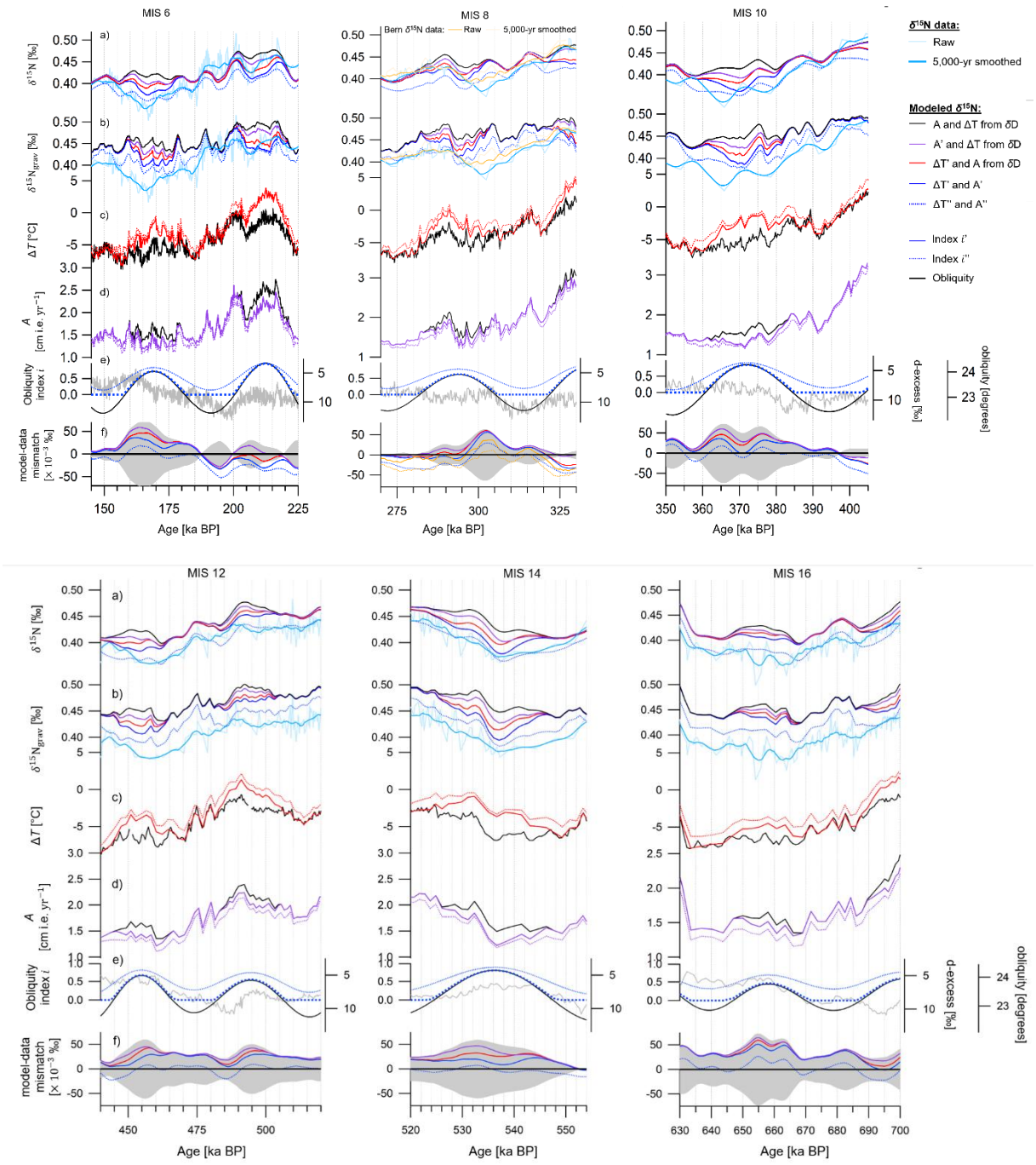

Figure S7 *Reconciling modeled $\delta^{15}N$ with data between 800 and 100 ka using an obliquity index to modulate past reconstructions of snow accumulation rate and temperature. a) $\delta^{15}N$ data (light blue) and smoothed over 5,000 years (cyan). Over MIS 8, $\delta^{15}N$ (light orange) and smoothed (orange) data measured at the University of Bern is shown. The modeled $\delta^{15}N$ is obtained using (1) temperature of Landais et al.[6] and snow accumulation rate of Bouchet et al.[15] (black); (2) temperature of Landais et al.[6] and snow accumulation rate modulated by obliquity with index i' (purple); (3) temperature modulated by obliquity with index i' and snow accumulation rate of Bouchet et al.[15] (red); (4) temperature and snow accumulation modulated by obliquity with index i' (dark blue); and (5) with index i'' (dark blue dots). b) $\delta^{15}N$ raw data (light blue) and smoothed over 5,000 years (cyan). The modeled gravitational component of $\delta^{15}N$ is shown for simulations (1) to (5). c) Temperature anomaly of Landais et al.[6] (ΔT; black) and modulated by obliquity ($\Delta T + 4i'$; red plain line) and ($\Delta T + 4i''$; red dotted line). d) Snow*

accumulation rate of Bouchet et al.[15] (A; black) and modulated by obliquity (A – 0.35i′; purple plain line) and (A – 0.35i″; purple dotted line). e) d-excess on reversed y-axis (gray line; right-hand side); obliquity index i′ varying between 0 (obliquity lower than its mid-value of 23.3°) and 1 (obliquity maximum = 24.5°) (blue dashed line; left-hand side); obliquity index i″ varying between 0 (obliquity minimum = 22.1°) and 1 (obliquity maximum = 24.5°) (blue dotted line; left-hand side) and obliquity (black line; right-hand side). f) $\delta^{15}N$ model-data mismatch for configurations (i) (gray envelop); (ii) (purple); (iii) (red); (iv) (dark blue) and (v) (dark blue dots). $\delta^{15}N$ model-data mismatch including Bern measurements for configurations (iv) (orange) and (v) (orange dots).

***Supplementary Section 7*: Seasonal bias in the EDC $\delta^{15}N$ data**

Severinghaus et al. [27] suggested that thermally driven convection in the firn could lead to anomalous thermal diffusion during winter creating bias in the classical way variations of $\delta^{15}N$ and $\delta^{40}Ar$ are interpreted through the gravitational and thermal fractionation. This idea was later revisited by Morgan et al. [28]. Both studies relied on measurements of $\delta^{15}N$ and $\delta^{40}Ar$ at South Pole either in the open firn porosity[27] or in the ice core[28]. While the first study could not provide direct evidence of a rectifier effect, the combination of $\delta^{15}N$ and $\delta^{40}Ar$ in the $\delta^{15}N$-excess (= $\delta^{15}N - \delta^{40}Ar/4$) suggests that a rectifier effect can be at play at some periods since the reconstructed ΔT evolution is far from the one expected from a surface temperature evolution based on δD profile and heat diffusion in the firn.

In the wake of these earlier studies, it may be argued that a seasonal bias would explain the deviation of the measured $\delta^{15}N$ compared to the modeled signal. Combined measurements of $\delta^{15}N$ and $\delta^{40}Ar$ and noble gas isotopic ratios were provided over deglaciations in Grimmer et al.[5]. The results are quite scattered with differences in the reconstructions performed by different isotopic combinations. Over the last 4 terminations, they found a relatively strong negative ΔT (-4°C) which gives support for the existence of a seasonal rectifier effect, much stronger than what was suggested at South Pole or Dome Fuji[28].

Data over MIS6 shows top–bottom firn temperature differences of about -5°C with maximum variations of 2°C. Variations of 2°C would lead to $\delta^{15}N$ variations of about 30 permeg, which is a third of the decline observed in the EDC record over glacial periods at high obliquity. Moreover, even if we are missing $\delta^{40}Ar$ data over the whole MIS 6, the variability in the reconstructed ΔT over MIS 6 does not appear to follow that of $\delta^{15}N$ between 140 and 160 ka (Figure S8). Based on these observations, we conclude that the thermal rectifier effect is probably not explaining the strong negative $\delta^{15}N$ excursion observed at high obliquity during glacial period.

but can be interpreted as top–bottom firn temperature differences of about -4°C with maximum variations of 2°C. Variations of 2°C would lead to δ^{15}N variations of about 30 permeg, which is a third of the decline observed in the EDC record over glacial periods at high obliquity. Moreover, even if we are missing δ^{40}Ar data over the whole MIS 6, the variability in the reconstructed ΔT over MIS 6 does not appear to follow that of δ^{15}N between 140 and 160 ka (Figure S8). Based on these observations, we conclude that the thermal rectifier effect is probably not explaining the strong negative δ^{15}N excursion observed at high obliquity during glacial period.

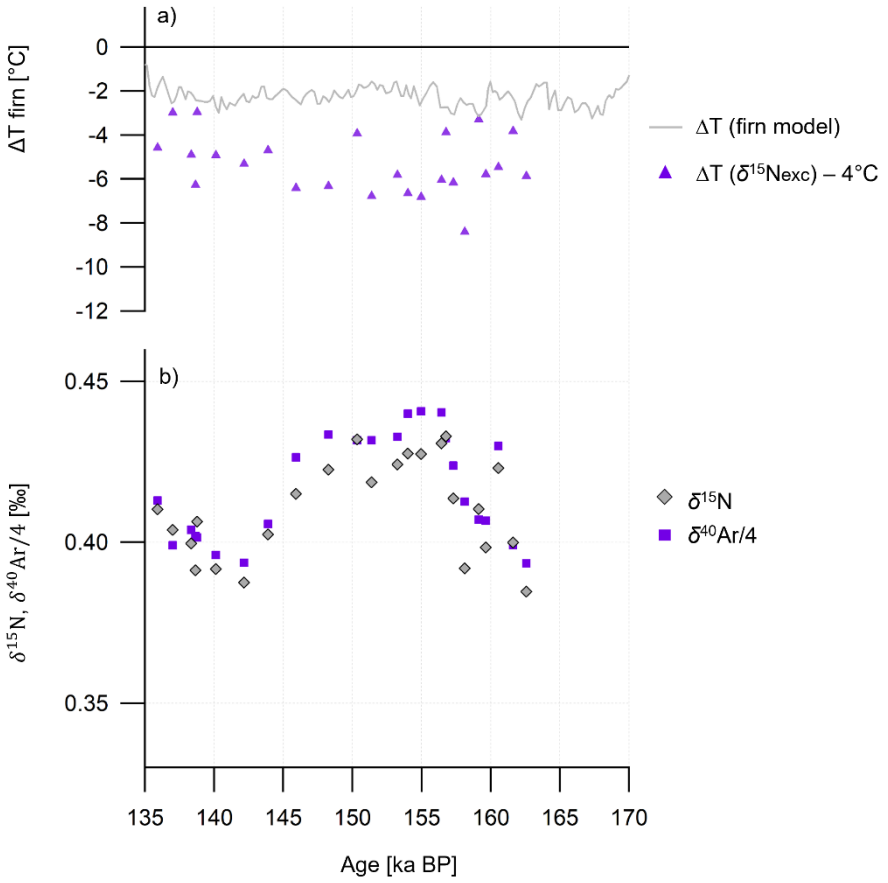

Fig. S8 *Evolution of the top-bottom firn temperature difference determined using EDC ice core measurements of $\delta^{15}N$ and $\delta^{40}Ar$ from the University of Bern. a) Firn temperature difference between top and bottom of the diffusive column. It can be calculated from the data as per $\Delta T = (\delta^{15}N - \delta^{40}Ar/4) / (\Omega^{15/14} - \Omega^{40/36}/4)$ where $\Omega^{a/b}$ is the empirically measured thermal diffusion sensitivity of the isotope pair a and b, and a kinetic fractionation correction calculated from Xe and Kr data from Grimmer et al. (2025) (purple triangles). The firn temperature difference can also be calculated from the firn model (test B) (grey line). b) $\delta^{15}N$ and $\delta^{40}Ar/4$ data from the University of Bern (respectively grey diamonds and purple squares[5]).*

References

1. Landais, A. *et al.* Firn-air δ15N in modern polar sites and glacial–interglacial ice: a model-data mismatch during glacial periods in Antarctica? *Quat Sci Rev* 25, 49–62 (2006).

2. Dreyfus, G. B. *et al.* Firn processes and δ15N: potential for a gas-phase climate proxy. *Quat Sci Rev* 29, 28–42 (2010).

3. Bréant, C., Martinerie, P., Orsi, A., Arnaud, L. & Landais, A. Modelling firn thickness evolution during the last deglaciation: constraints on sensitivity to temperature and impurities. *Climate of the Past* 13, 833–853 (2017).

4. Bréant, C. *et al.* Unveiling the anatomy of Termination 3 using water and air isotopes in the Dome C ice core, East Antarctica. *Quat Sci Rev* 211, 156–165 (2019).

5. Grimmer, M. *et al.* AMOC Modulates Ocean Heat Content During Deglaciations. *Geophys Res Lett* 52, e2024GL114415 (2025).

6. Landais, A. *et al.* Interglacial Antarctic–Southern Ocean climate decoupling due to moisture source area shifts. *Nature Geoscience 2021 14:12* 14, 918–923 (2021).

7. Caillon, N., Jouzel, J., Severinghaus, J. P., Chappellaz, J. & Blunier, T. A novel method to study the phase relationship between Antarctic and Greenland climate. *Geophys Res Lett* 30, (2003).

8. Parrenin, F. *et al.* On the gas-ice depth difference (Δdepth) along the EPICA Dome C ice core. *Climate of the Past* 8, 1239–1255 (2012).

9. Veres, D. *et al.* The Antarctic ice core chronology (AICC2012): an optimized multi-parameter and multi-site dating approach for the last 120 thousand years. *Climate of the Past* 9, 1733–1748 (2013).

10. Bazin, L. *et al.* An optimized multi-proxy, multi-site Antarctic ice and gas orbital chronology (AICC2012): 120–800 ka. *Climate of the Past* 9, 1715–1731 (2013).

11. Arnaud, L., Barnola, J. M. & Duval, P. Physical modeling of the densification of snow/firn and ice III the upper part of polar ice sheets. (2000).

12. Herron, M. M. & Langway, C. C. Firn densification: an empirical model. *Journal of Glaciology* 25, (1980).

13. Masson-Delmotte, V. *et al.* A Review of Antarctic Surface Snow Isotopic Composition: Observations, Atmospheric Circulation, and Isotopic Modeling. *J Clim* 21, 3359–3387 (2008).

14. Buizert, C. *et al.* Antarctic surface temperature and elevation during the Last Glacial Maximum. *Science (1979)* 372, 1097–1101 (2021).

15. Bouchet, M. *et al.* The Antarctic Ice Core Chronology 2023 (AICC2023) chronological framework and associated timescale for the European Project for Ice Coring in Antarctica (EPICA) Dome C ice core. *Climate of the Past* 19, 2257–2286 (2023).

16. Quiquet, A., Dumas, C., Ritz, C., Peyaud, V. & Roche, D. M. The GRISLI ice sheet model (version 2.0): calibration and validation for multi-millennial changes of the Antarctic ice sheet. *Geosci Model Dev* 11, 5003–5025 (2018).

17. Lambert, F., Bigler, M., Steffensen, J. P., Hutterli, M. & Fischer, H. Centennial mineral dust

variability in high-resolution ice core data from Dome C, Antarctica. *Climate of the Past* 8, 609–623 (2012).

18. Goosse, H. *et al.* Description of the Earth system model of intermediate complexity LOVECLIM version 1.2. *Geosci Model Dev* 3, 603–633 (2010).

19. Berger, AndréL. Long-Term Variations of Daily Insolation and Quaternary Climatic Changes. *Journal of Atmospheric Sciences* 35, 2362–2367 (1978).

20. Köhler, P., Nehrbass-Ahles, C., Schmitt, J., Stocker, T. F. & Fischer, H. A 156 kyr smoothed history of the atmospheric greenhouse gases CO2, CH4, and N2O and their radiative forcing. *Earth Syst Sci Data* 9, 363–387 (2017).

21. Menviel, L. *et al.* The penultimate deglaciation: protocol for Paleoclimate Modelling Intercomparison Project (PMIP) phase 4 transient numerical simulations between 140 and 127ka, version 1.0. *Geosci Model Dev* 12, 3649–3685 (2019).

22. Menviel, L. *et al.* Drivers of the evolution and amplitude of African Humid Periods. *Communications Earth & Environment 2021 2:1* 2, 237- (2021).

23. Abe-Ouchi, A. *et al.* Insolation-driven 100,000-year glacial cycles and hysteresis of ice-sheet volume. *Nature* 500, 190–193 (2013).

24. Menviel, L., England, M. H., Meissner, K. J., Mouchet, A. & Yu, J. Atlantic-Pacific seesaw and its role in outgassing CO2 during Heinrich events. *Paleoceanography* 29, 58–70 (2014).

25. Peltier, W. R. & Vettoretti, G. Dansgaard-Oeschger oscillations predicted in a comprehensive model of glacial climate: A “kicked” salt oscillator in the Atlantic. *Geophys Res Lett* 41, 7306–7313 (2014).

26. Menviel, L., Timmermann, A., Timm, O. E. & Mouchet, A. Deconstructing the Last Glacial termination: the role of millennial and orbital-scale forcings. *Quat Sci Rev* 30, 1155–1172 (2011).

27. Severinghaus, J. P., Grachev, A. & Battle, M. Thermal fractionation of air in polar firn by seasonal temperature gradients. *Geochemistry, Geophysics, Geosystems* 2, (2001).

28. Morgan, J. D. *et al.* Gas isotope thermometry in the South Pole and Dome Fuji ice cores provides evidence for seasonal rectification of ice core gas records. *Cryosphere* 16, 2947–2966 (2022).